Hindawi Publishing Corporation
Journal of Spectroscopy
Volume 2015, Article ID 940172, 8 pages
http://dx.doi.org/10.1155/2015/940172

Research Article

Raman and Fluorescence Spectroscopy of CeO_2, Er_2O_3, Nd_2O_3, Tm_2O_3, Yb_2O_3, La_2O_3, and Tb_4O_7

Jianlan Cui and Gregory A. Hope

Queensland Micro- and Nanotechnology, School of Natural Sciences, Griffith University, Nathan, QLD 4111, Australia

Correspondence should be addressed to Gregory A. Hope; g.hope@griffith.edu.au

Received 14 January 2015; Revised 5 April 2015; Accepted 7 April 2015

Academic Editor: Eugen Culea

To better understand and ascertain the mechanisms of flotation reagent interaction with rare earth (RE) minerals, it is necessary to determine the physical and chemical properties of the constituent components. Seven rare earth oxides (CeO_2, Er_2O_3, Nd_2O_3, Tm_2O_3, Yb_2O_3, La_2O_3, and Tb_4O_7) that cover the rare earth elements (REEs) from light to heavy REEs have been investigated using Raman spectroscopy. Multiple laser sources (wavelengths of 325 nm, 442 nm, 514 nm, and 632.8 nm) for the Raman shift ranges from 100 cm^{-1} to 5000 cm^{-1} of these excitations were used for each individual rare earth oxide. Raman shifts and fluorescence emission have been identified. Theoretical energy levels for Er, Nd, and Yb were used for the interpretation of fluorescence emission. The experimental results showed good agreement with the theoretical calculation for Er_2O_3 and Nd_2O_3. Additional fluorescence emission was observed with Yb_2O_3 that did not fit the reported energy level diagram. Tb_4O_7 was observed undergoing laser induced changes during examination.

1. Introduction

The success of mineral flotation is contingent upon the interfacial interaction between the collector(s) and the mineral surface. In order to characterize and ascertain the mechanisms of flotation reagent interaction with rare earth (RE) minerals, it is necessary to determine the physical and chemical properties of the constituent components.

Rare earth oxides (REOs) are the most important components of RE minerals. Each individual REO has different vibrational and electronic properties including Raman and fluorescence spectra. There have been a number of papers published for the characterization of REOs using Raman spectroscopy [1–6]. Tucker et al. reported three REOs (Eu_2O_3, Dy_2O_3, and Tm_2O_3) using multiple laser sources. Most of the studies have used one laser source and the identification of Raman bands from fluorescence emissions is often ambiguous. Raman spectroscopy and fluorescent emissions are valuable techniques for identifying the interactions in the RE minerals flotation system [7]. The fundamental physics studies of REO fluorescence are not readily appreciated by mineral technologists, and there is a need for presenting the data to these investigators in a clear and unified way. Systematic investigation using multiple radiation sources has been undertaken in this study. In addition, the Raman spectroscopic studies related to crystal structural analysis were undertaken in wavenumber region between 100 cm^{-1} and 2000 cm^{-1}. The Raman spectra regions for wavenumber above 3500 cm^{-1} have not been reported for Nd_2O_3 and La_2O_3.

For the present study, 7 REOs including La_2O_3, CeO_2, Nd_2O_3, Yb_2O_3, Er_2O_3, Tm_2O_3, and Tb_4O_7 were investigated with Raman spectroscopy and for fluorescence emission. These REOs cover the rare earth elements (REEs) from light to heavy REEs. The most common RE mineral, bastnaesite, is rich in Ce and La [8, 9] while Nd and Er have been widely applied in different industries. The less common Tm and Yb are also important due to the increasing interest in the heavy REEs as they have not been fully investigated. Tb is a unique RE that has been reported to form mixed valence compounds with a nonstoichiometric structure [10]. Fundamental characterization of these REOs is important

for better understanding the properties of the REs and exploring new applications. This study has adopted multiple radiation sources (wavelengths of 325 nm, 442 nm, 514 nm, and 632.8 nm) in investigating the wavenumber of the Raman shift ranges from 100 cm^{-1} to 5000 cm^{-1} of these excitations.

2. Materials and Methods

2.1. Materials. Cerium oxide (CeO_2), erbium oxide (Er_2O_3), neodymium oxide (Nd_2O_3), thulium oxide (Tm_2O_3), ytterbium oxide (Yb_2O_3), lanthanum oxide (La_2O_3), and terbium oxide (Tb_4O_7) were purchased from Sigma-Aldrich. The samples were investigated as supplied powder form.

2.2. Vibrational Spectroscopy. All the Raman spectra were recorded on a Renishaw inVia spectrometer. The excitation sources were 325 nm (HeCd laser), 442 nm (HeCd laser), 514.5 nm (Ar ion laser), and 632.8 nm (HeNe laser). The scattered light was detected with a Peltier-cooled CCD detector (Renishaw) with spectral resolution ~ 2 cm^{-1}. The chip contains 1024 × 256 active pixels. The manufacturer specified a quantum efficiency of approximately 43% at a wavelength of 633 nm and a 100% fill factor rating to maximize sensitivity. The read-out noise of the CCD is 4 RMS electrons per pixel. The white light response curve obtained for the CCD chip was similar to the reference by other CCD manufactures [11]. Raman spectra were calibrated using the 520 cm^{-1} silicon band. The spectra were recorded in both wavenumbers and wavelengths. Spectral manipulations such as baseline adjustment, smoothing, and normalization were performed with the WiRE 3.3 software (Renishaw, UK).

3. Results and Discussion

Most REEs (in this study Er, Nd, Tm, Yb, and La) exhibit 3^+ oxidation states in their compounds and sesquioxides are usually observed. Ce is stable in its 4^+ oxidation state while Tb oxide has been reported as a mixed valence compound [12]. In addition, polymorphism has been observed for the sesquioxides and five different crystalized types (A, B, C, H, and X) were reported [1]. C type sesquioxides are formed under room temperature and would transform to other phases with different conditions [1, 13]. It is expected that Raman spectra with a similar band pattern would be obtained from RE sesquioxides having the same crystal structure. Fluorescence emissions with RE compounds are commonly observed overlapping the Raman spectra. Typical strong fluorescing REOs include Er and Nd. It is important to identify the origin of the various bands/lines presented in the Raman spectra. Using a range of excitation energy is an effective method to distinguish the Raman bands from fluorescence emission. Theoretical energy levels for Er, Nd, and Yb were also utilized for the interpretation of fluorescence emission.

3.1. Cerium Oxide (CeO_2). CeO_2 has the fluorite type cubic crystal structure that exhibits only one allowed Raman mode, T_2g. It emanates from the Ce-O-Ce symmetric vibration [4, 14]. In the present study, the Raman spectra from 442 nm, 514 nm, and 633 nm excitation were consistent, having a single Raman band observed at a shift of 465 cm^{-1} (Figure 1). The spectrum is consistent with that reported by several authors and the band at 465 cm^{-1}has been assigned to the first order scattering [4, 5, 15]. No fluorescence emissions were observed in the spectra (Figure 2).

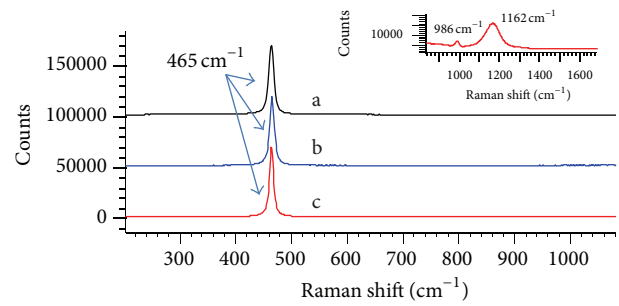

FIGURE 1: Raman band for CeO_2 with (a) 442 nm excitation, (b) 514 nm excitation, and (c) 633 nm excitation. A strong band at 465 cm^{-1} shift was observed with the three excitation sources.

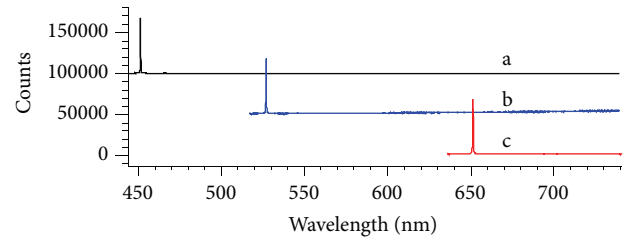

FIGURE 2: Emission spectra for CeO_2 with (a) 442 nm excitation, (b) 514 nm excitation, and (c) 633 nm excitation. The emissions lines present are from the Raman band at 465 cm^{-1} shift.

The second order scattering bands have been reported by other authors at 983 cm^{-1}, 1030 cm^{-1}, and 1160 cm^{-1} [15]. In this study, low intensity bands at 986 cm^{-1} and 1162 cm^{-1} were observed, which can be attributed to this mode (Figure 1, top right figure). Weber et al. have conducted a comprehensive study on the Raman second order scattering on CeO_2. The authors concluded that there were a number of bands ranging from 264 cm^{-1} to 1180 cm^{-1} that emanate from the second order scattering. These bands resulted from different phonon symmetry modes [5]. For example, the band observed at the present study at 986 cm^{-1} emanated from the combination of the A_1g, Eg, and F_2g modes. The band near 1180 cm^{-1} (in this study, the band was observed at 1162 cm^{-1}) was assigned to a 2LO mode rather than single critical point phonon overtone (Table 1).

The band positions (including first order and second order scattering) varied from 1 cm^{-1} to 20 cm^{-1} from those reported by previous investigators. Denning and Ross proposed that a number of factors contribute to changes of the Raman band position including phonon confinement, strain, particle size effect, and defects [16]. Raman band shifts caused by differences in particle sizes have been reported by a number of authors [5, 14, 19]. Differences in particle size have

Table 1: Band positions and corresponding Raman modes for REOs.

Band position (cm^{-1})	Raman mode	REO	Reference
465	T_2g	CeO_2	[4, 12]
986	$A_1g + Eg + F_2g$	CeO_2	[5]
1162	2LO	CeO_2	[5]
472	A_2u	Nd_2O_3	[16]
384	Ag + Fg	Tm_2O_3	[1, 17]
365	Ag + Fg	Yb_2O_3	[1, 18]
444	Eg	Ld_2O_3	[16]

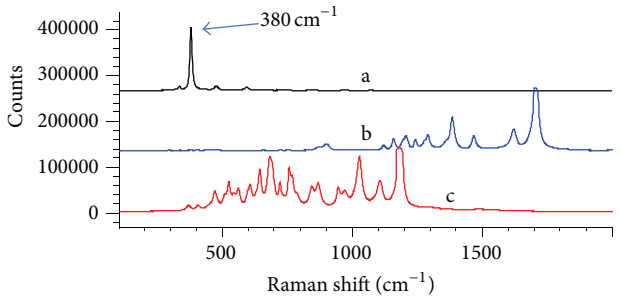

Figure 3: Spectra obtained from Er_2O_3 using (a) 442 nm excitation, (b) 514 nm excitation, and (c) 633 nm excitation, presented as Raman shifts.

led to variation in phonon relaxation and thus caused band position shifts in the lattice area of the spectra [19].

The intensities of the T_2g Raman bands are above 65,000 in counts when excited with less than 0.006 mW of power output and could easily be saturated (the same effect was observed for the three lasers used). This is an unusually strong signal for a normal Raman spectrum using the Renishaw instrument. Similar observations have also been reported with other fluorite type structure compounds; for example, Mead reported that low gain settings were required for CaF_2, BaF_2, SrF_2, and $SrCl_2$ compounds due to the strong scattering effect [20]. It is suggested that the fluorite type cubic crystal structure generates intense Raman scattering.

3.2. Erbium Oxide (Er_2O_3). Er is commonly used as a laser source material and it has been well characterized for its fluorescence properties [21, 22]. The Raman and emission spectra observed from Er_2O_3 are present in Figures 3 and 4.

No Raman bands were observable in the three spectra (Figure 3). It is probable that the Raman bands were either overlapped by the fluorescence emission or were too weak to be observed in the presence of the strong fluorescence effect. For most REOs, the Raman bands are usually present between 100 cm^{-1} and 1000 cm^{-1}. With the Er_2O_3 sample, the fluorescence lines were coincidentally shown in this area (or near this area) when the spectra were plotted as wavenumbers.

In the emission spectra from 640 nm to 700 nm and from 530 nm to 580 nm, the emission lines show good agreement in both line shapes and wavelength position between the three sets of excitations spectra (Figures 4 and 5). The intensities

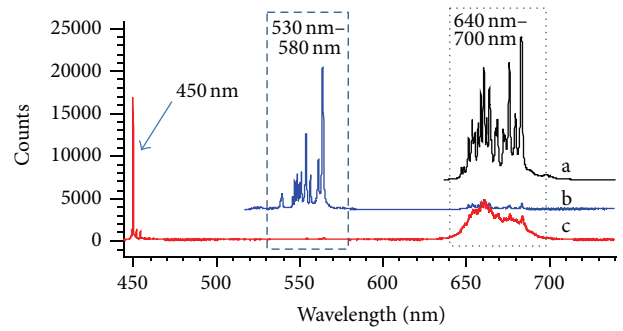

Figure 4: Emission spectra from Er_2O_3 using (a) 633 nm excitation, (b) 514 nm excitation, and (c) 442 nm excitation.

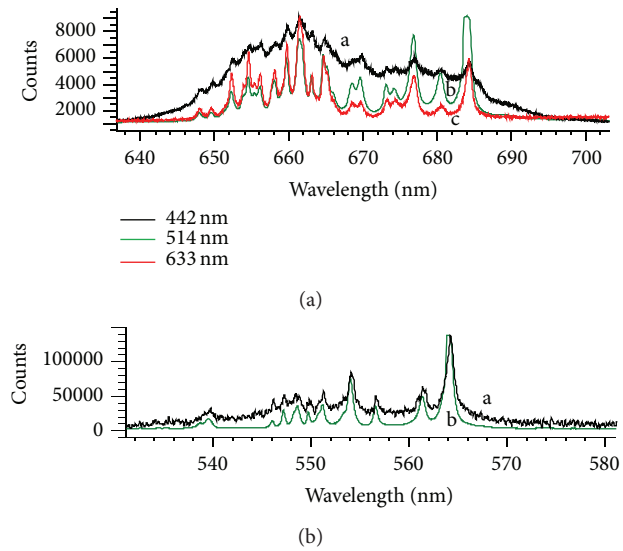

Figure 5: Fluorescence emission spectra for Er_2O_3 with 442 nm excitation (a), 514 nm excitation (b), and 633 nm excitation (c) in the ranges of (1) 640 nm–700 nm and (2) 530 nm–580 nm. The emission lines exhibit good agreement in emission positions for different excitation wavelengths.

vary between different excitations, due to the variation of excitation laser power. It can be confirmed that the lines are sourced from fluorescence emissions from the Er(III) [23]. An intense band together with a number of small emissions is exhibited for the 442 nm emission spectra at 450 nm. These lines are also observed at 380 cm^{-1} in the Raman spectrum. They are assigned to fluorescence emissions.

Electrons can be excited to different energy levels, and they can emit photons during relaxation. A theoretical energy level diagram for Er(III) is shown in Figure 6. The experimental results in the present study are consistent with the theoretical value presented by Wu et al., allowing for some relaxation processes [22]. The transition at 650 nm is due to the electronic transition from $^4F_{9/2} \rightarrow {}^4I_{15/2}$. Similarly, the emissions observed in Figures 4 and 5 (bottom figure) from 530 nm to 580 nm are expected to result from relaxation and emission from a higher energy level excited state ($^4S_{3/2} \rightarrow {}^4I_{15/2}$).

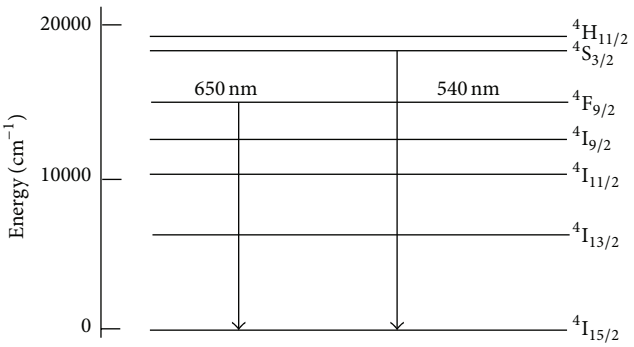

FIGURE 6: Energy level for Er^{3+}, data sourced from Yu et al. [18].

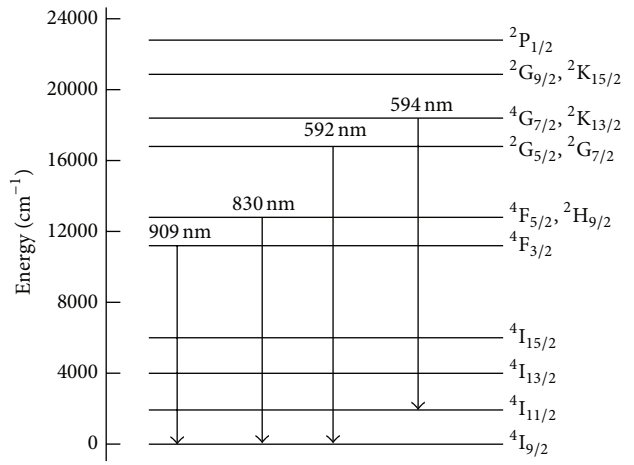

FIGURE 7: Energy level diagram of Nd(III) [19].

3.3. Neodymium Oxide (Nd_2O_3). A theoretical energy level diagram of Nd(III) is presented in Figure 7 [19]. A number of fluorescence emissions were expected in the emission spectra from the Raman laser excitation. For example, emissions of 592 nm and 594 nm corresponding to $^4G_{5/2}$, $^2G_{7/2} \rightarrow {}^4I_{9/2}$ and $^4G_{7/2}$, $^2K_{13/2} \rightarrow {}^4I_{11/2}$ were expected when using the 514 nm wavelength as excitation.

Figure 8 presents the fluorescence emission spectra obtained using four different excitation wavelengths (325 nm, 442 nm, 514 nm, and 633 nm). The emissions from 860 nm to 900 nm using the 633 nm excitation are in good agreement with the transition from $^4F_{3/2} \rightarrow {}^4I_{9/2}$ and $^4F_{5/2}$, $^2H_{9/2} \rightarrow {}^4I_{9/2}$. The electronic transition corresponding to 592 nm and 594 nm ($^4G_{5/2}$, $^2G_{7/2} \rightarrow {}^4I_{9/2}$ and $^4G_{7/2}$, $^2K_{13/2} \rightarrow {}^4I_{11/2}$) was also displayed in spectrum where 514 nm excitation was used. When higher energy excitation was utilized (442 nm and 325 nm), no emissions were observed in the range of 580 nm–720 nm. It is likely that the electrons were excited to a much higher energy level and relaxed through a different pathway compared to when the 514 nm wavelength was used, and the emission was out of the detection range of the equipment.

Under room temperature, Nd_2O_3 powder was reported having an A type phase crystal structure, but sometimes a combination of C type phase could exist [1, 13]. Four phonon

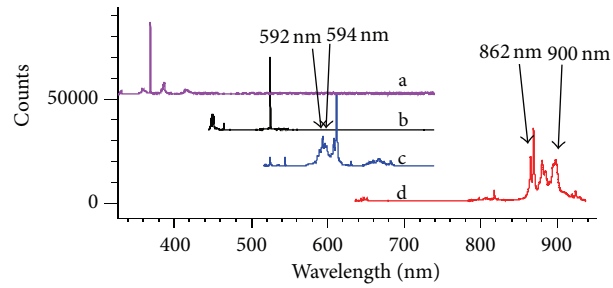

FIGURE 8: Fluorescence emissions for Nd_2O_3 by using (a) 325 nm, (b) 442 nm, (c) 514 nm, and (d) 633 nm excitations.

modes ($2A_2u + 2Eu$) were expected for the A type crystal [1]. The irreducible representations for the C type crystal optical and acoustical modes are

$$\Gamma op = 4Ag + 4Eg + 14Fg + 5A_2u + 5Eu + 16Fu,$$
$$\Gamma ac = Fu, \quad (1)$$

where 22 Raman bands (Ag, Eg, and Fg) are predicted in the lower wavenumber area [6, 17]. However, none of the reported spectra in literature has shown all the predicted bands. Heiba attributed this to the accidental degeneracies or low Raman scattering cross sections of the corresponding vibrations [17]. In the present study, the Raman spectra with excitation of 442 nm and 633 mm were identical. Fluorescent emissions were observed overlapping the Raman spectrum in the lattice area with the 514 nm excitation (Figure 9). Four Raman bands were observed at 296 cm^{-1}, 362 cm^{-1}, 387 cm^{-1}, and 472 cm^{-1}. The band at 472 cm^{-1} has been assigned to the A_2u mode [16] (Table 1). Ubaldini and Carnasciali who synthesized the Nd_2O_3powder with C type crystal structure from $Nd(OH)_3$ reported a number of different bands from the current study in the lattice area [1]. Two types of crystals present in the Nd_2O_3 powder used for this study could be responsible for the different observations in the two studies. In addtion, the X-ray photoelectron spectroscopy (XPS) has confirmed Nd carbonate and Nd hydroxide were present at the surface. The sharp band at 3598 cm^{-1} assigned to νO-H also supports the existence of Nd hydroxide. Surface hydroxylation and carbonation have contributed to complicated Raman spectra and it is difficult to identify the assignments in the lattice area.

3.4. Thulium Oxide (Tm_2O_3). Tm_2O_3 powder is reported having a C type cubic structure at room temperature [1]. Similar to other C type structure REOs, not all predicted bands were observed. In the present study, four Raman bands, 336 cm^{-1}, 384 cm^{-1}, 484 cm^{-1}, and 602 cm^{-1}, were observed in the spectra obtained with the three excitations (Figure 10). Comparison of the wavenumber shift and energy plots confirms these are Raman bands. Figure 11 presents the emission data for three wavelengths, which is consistent with the strong Raman spectra observed, with very weak (or no) fluorescence bands evident in the spectra. Using 633 nm laser excitation, Ubaldini and Carnasciali reported the most

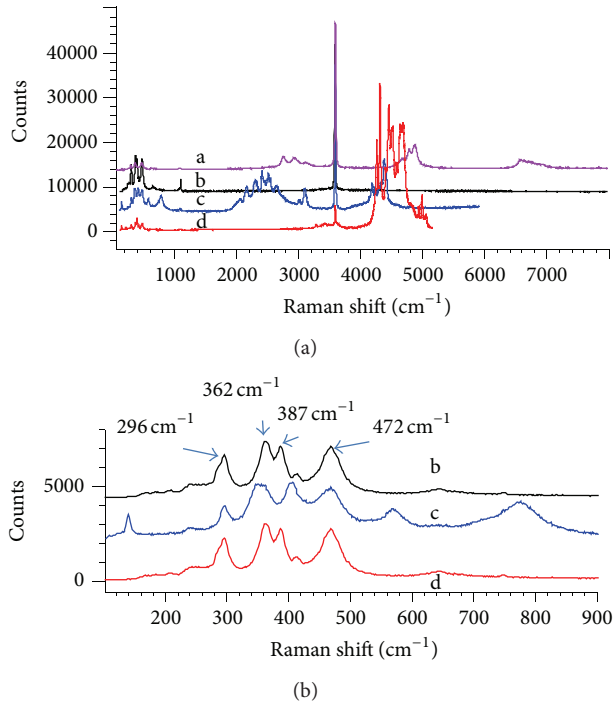

FIGURE 9: Raman spectra for Nd_2O_3 by using (a) 325 nm, (b) 442 nm, (c) 514 nm, and (d) 633 nm excitations. Top: scanning range from 100 cm^{-1} to 8000 cm^{-1}; bottom: scanning range from 100 cm^{-1} to 1000 cm^{-1}.

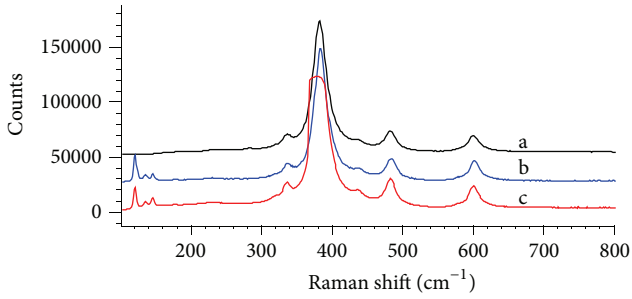

FIGURE 10: Raman spectra for Tm_2O_3 with (a) 442 nm excitation, (b) 514 nm excitation, and (c) 633 nm excitation.

intense Raman band was at 383 cm^{-1} while another two bands were at 482 cm^{-1} and 601 cm^{-1} [1]. The spectra obtained in this study were consistent with those that Ubaldini and Carnasciali reported. The strongest band at 384 cm^{-1} has been assigned to the Ag mode or the combination mode of Ag and Fg [1, 17] (Table 1).

Bilijan also reported broad ranges of Raman bands from 1000 cm^{-1} to 2000 cm^{-1} (1090 1140, 1303, 1377, 1593, and 1814 at cm^{-1}) and 3000 cm^{-1} to 3500 cm^{-1} (3217 and 3417 at cm^{-1}) using 1064 nm excitation [3]. These bands correspond to 1190 nm to 1351 nm and 1562 nm to 1695 nm for the emission spectra when using 1064 nm excitation. These emissions are out of the detection limit in the present study. The reported "Raman" bands were not observed with the three excitation wavelengths in the present study and it is likely that they

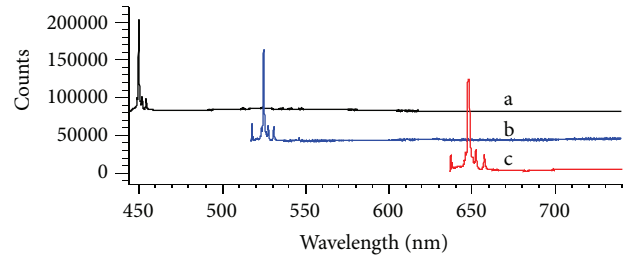

FIGURE 11: Fluorescence emission spectra for Tm_2O_3 with (a) 442 nm excitation, (b) 514 nm excitation, and (c) 633 nm excitation. Raman bands, being Raman shifts, appear at different wavelengths in the emission spectra.

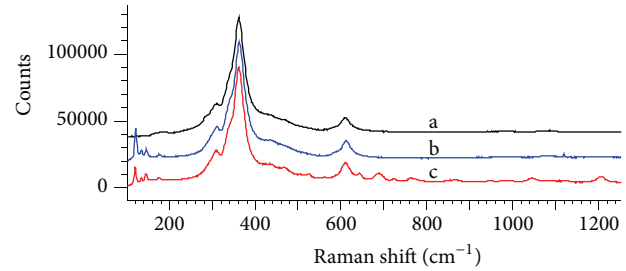

FIGURE 12: Raman spectra for Yb_2O_3 with (a) 442 nm excitation, (b) 514 nm excitation, and (c) 633 nm excitation.

were fluorescence bands from $^3H_5 \rightarrow {}^3H_6$ and $^3F_4 \rightarrow {}^3H_6$ transitions.

3.5. Ytterbium Oxide (Yb_2O_3). The most intense Raman band, observed at 365 cm^{-1}, was evident at all three excitations for the Yb_2O_3 sample (Figure 12). This band can be attributed to the combination mode of Ag and Fg [1, 18] (Table 1).

A number of small bands near 620 cm^{-1} were shown in the 633 nm spectrum. These bands correspond to 662 nm to 685 nm in the emission spectrum (Figure 13). The emissions are in good agreement with the 514 nm excitation spectrum. It indicates that they are fluorescence lines. These emissions have not been reported in the literature. The general agreement is that Yb^{3+} has a simple energy diagram consisting of three crystal field levels in the excited $2F_{5/2}$ manifold and four in the $2F_{7/2}$ ground state manifold [3, 24]. The transition between these two states is corresponding to the 980 nm emission. However, the observation for the Yb_2O_3 emission spectrum does not agree with this energy level diagram, with which only transition $2F_{5/2} \rightarrow 2F_{7/2}$is predicted. It supports that additional transition exists (even though it is not strong), allowing the 662 nm–685 nm emission to occur.

3.6. Lanthanum Oxide (La_2O_3). In the present study, four bands at 451 cm^{-1}, 341 cm^{-1}, 283 cm^{-1}, and 271 cm^{-1} were observed at all excitations (Figure 14). These bands have been identified as Raman bands. No fluorescence emissions were observed (Figure 15).

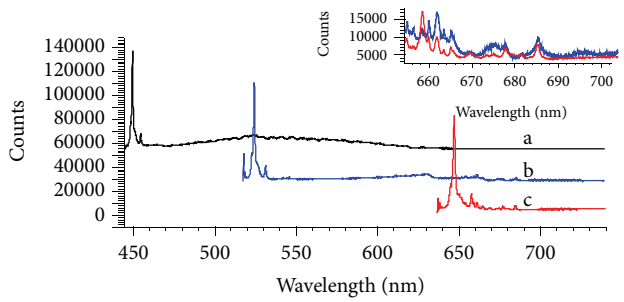

Figure 13: Emissions spectra for Yb_2O_3 with (a) 442 nm excitation, (b) 514 nm excitation, and (c) 633 nm excitation. The 514 nm (blue) and 633 nm (red) spectra range from 650 nm to 700 nm is shown on the top right corner.

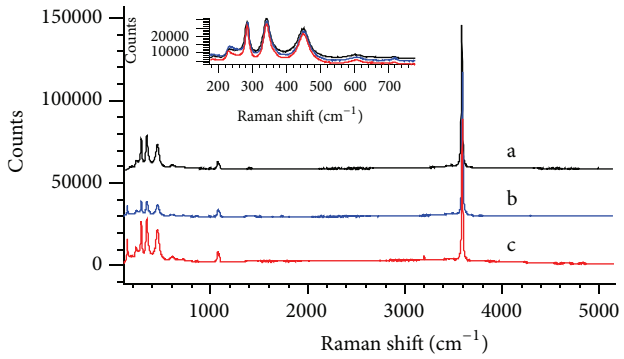

Figure 14: Raman spectra for La_2O_3 with (a) 442 nm excitation, (b) 514 nm excitation, and (c) 633 nm excitation. The spectra ranges from 200 nm to 750 cm^{-1} are shown on the small figure. From top to bottom: 442 nm excitation, 514 nm excitation, and 633 nm excitation.

Different theoretical and experimental Raman shifts have been reported in the literature [1, 16]. The band at 451 cm^{-1} is assigned to the Eg ν1 mode and is consistent with that observed by Denning and Ross (Table 1). The authors also employed the FG matrix method for the theoretical band positions and predicted that the Eg ν1 mode would occur at 449 cm^{-1} [16]. The calculation is in good agreement with the present study. Other Raman bands (341 cm^{-1}, 283 cm^{-1}, and 271 cm^{-1}) observed in the present work have not been reported previously. The Raman shifts reported by Boldish and White for their La_2O_3 sample, 410 cm^{-1} and 195 cm^{-1}, were not observed in the present study [2]. Similar to Nd_2O_3, the spectra of La_2O_3 from powder samples would include a couple of crystal orientations and would be different from single crystal spectra [2]. Surface hydroxylation and carbonation also contribute to the differences in band position reported by different authors. The bands at 1074 cm^{-1}, 1092 cm^{-1}, and 3604 cm^{-1} support carbonate and hydroxide compounds present at the surface (Figure 14).

3.7. Terbium Oxide (Tb_4O_7). Tb_4O_7 has been reported as a mixed valence compound with nonstoichiometric structure [10]. It undergoes phase and structural changes when exposed

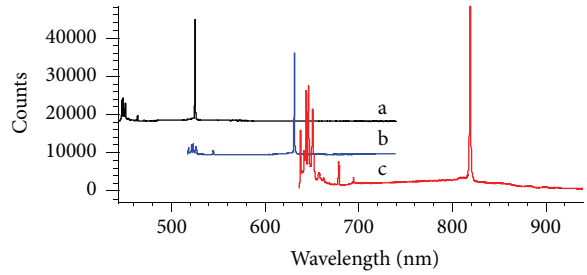

Figure 15: Emission spectra for La_2O_3 with (a) 442 nm excitation, (b) 514 nm excitation, and (c) 633 nm excitation.

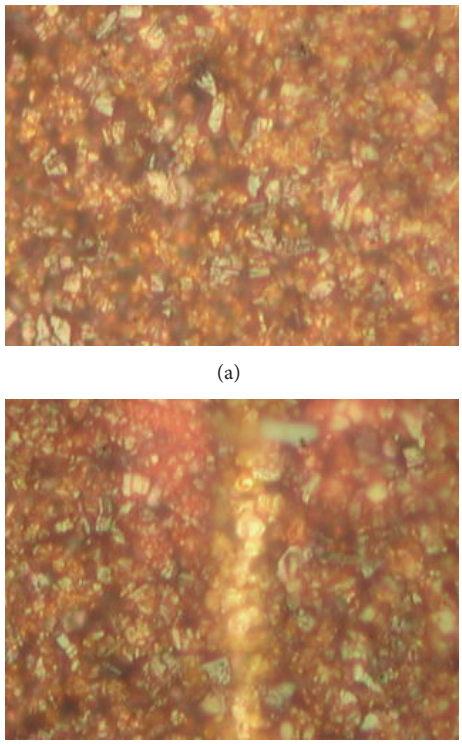

(a)

(b)

Figure 16: Images for Tb_4O_7 (a) before investigation using Raman spectroscopy and (b) after investigation using Raman spectroscopy. Excitation: 442 nm laser.

to an electron beam [25, 26]. In order to avoid structural change during examination, low intensity excitation radiation was adopted for this Raman spectroscopic study. Surface damage was observed in the samples at any of the laser wavelengths studied. Figure 16 shows the microscope images before and after the sample was excited using 442 nm excitation. The surface was uniform before the laser was introduced; following exposure, a bright strip was observed where the laser had been focused. Two orange areas next to the strip were also observed. It is likely that a phase transformation has occurred during the examination.

The Raman spectra from the sample changed with exposure time, as a result of the laser radiation induced changes. Figure 17 shows two acquired Raman spectra on the same

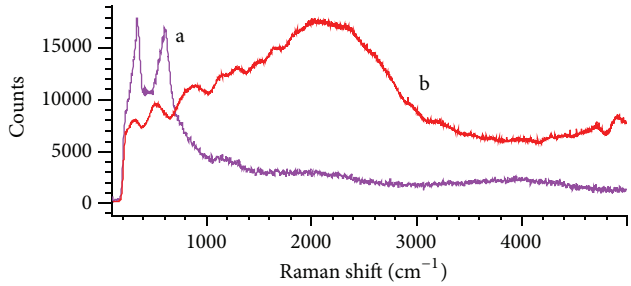

FIGURE 17: Raman spectra on the same spot for Tb_4O_7 (a) primary spectrum and (b) consecutive spectrum (excitation wavelength was 442 nm).

spot using 442 nm excitation. Both spectra were run under the same excitation conditions. The initial spectrum showed two bands at 352 cm^{-1} and 598 cm^{-1}; subsequently, these two bands broadened and shifted to 302 cm^{-1} and 502 cm^{-1}. A broad band that was observed from 1800 cm^{-1} to 3000 cm^{-1} also shifted to lower wavenumbers by 200 cm^{-1} and the spectrum started exhibiting a low signal to noise ratio.

4. Conclusion

Seven rare earth oxides (CeO_2, Er_2O_3, Nd_2O_3, Tm_2O_3, Yb_2O_3, La_2O_3, and Tb_4O_7) were characterized using Raman spectroscopy. Multiple radiation sources (wavelengths of 325 nm, 442 nm, 514 nm, and 632.8 nm) were used for each individual rare earth oxide and the Raman bands and fluorescence emissions have been identified. Strong fluorescence emissions were observed for Er_2O_3 and Nd_2O_3. Emissions from 662 nm to 685 nm were observed for Yb_2O_3, which did not agree with the energy level diagram. It is suggested that additional transition exists in Yb_2O_3, allowing these emission to occur. Tb_4O_7 was observed undergoing laser induced changes during examination.

Conflict of Interests

The authors declare that there is no conflict of interests regarding the publication of this paper.

Acknowledgments

The Australian Research Council and Griffith University Postgraduate Funding have provided support for this research project. This work was performed in part at the Queensland Node of the Australian National Fabrication Facility, a company established under the National Collaborative Research Infrastructure Strategy to provide nano- and microfabrication facilities for Australia's researchers.

References

[1] A. Ubaldini and M. M. Carnasciali, "Raman characterisation of powder of cubic RE_2O_3 (RE = Nd, Gd, Dy, Tm, and Lu), Sc_2O_3 and Y_2O_3," *Journal of Alloys and Compounds*, vol. 454, no. 1-2, pp. 374–378, 2008.

[2] S. I. Boldish and W. B. White, "Vibrational spectra of crystals with the A-type rare earth oxide structure—I. La_2O_3 and Nd_2O_3," *Spectrochimica Acta Part A*, vol. 35, no. 11, pp. 1235–1242, 1979.

[3] T. Biljan, S. Rončević, Z. Meić, and K. Kovač, "Non-vibrational features in NIR FT-Raman spectra of lanthanide sesquioxides," *Chemical Physics Letters*, vol. 395, no. 4–6, pp. 246–252, 2004.

[4] V. G. Keramidas and W. B. White, "Raman spectra of oxides with the fluorite structure," *The Journal of Chemical Physics*, vol. 59, no. 3, pp. 1561–1562, 1973.

[5] W. H. Weber, K. C. Hass, and J. R. McBride, "Raman study of CeO_2: second-order scattering, lattice dynamics, and particle-size effects," *Physical Review B*, vol. 48, no. 1, pp. 178–185, 1993.

[6] L. A. Tucker, F. J. Carney Jr., P. McMillan, S. H. Lin, and L. Eyring, "Raman and resonance Raman spectroscopy of selected rare-earth sesquioxides," *Applied Spectroscopy*, vol. 38, no. 6, pp. 857–860, 1984.

[7] J. Cui, G. A. Hope, and A. N. Buckley, "Spectroscopic investigation of the interaction of hydroxamate with bastnaesite (cerium) and rare earth oxides," *Minerals Engineering*, vol. 36-38, pp. 91–99, 2012.

[8] V. C. Farmer, *The Infrared Spectra of Minerals*, Mineralogical Society, London, UK, 1974.

[9] R. L. Frost and M. J. Dickfos, "Raman spectroscopy of halogen-containing carbonates," *Journal of Raman Spectroscopy*, vol. 38, no. 11, pp. 1516–1522, 2007.

[10] N. Imanaka, T. Masui, and Y. Woon Kim, "First electrochemical growth of $Tb_{16}O_{30}$ single crystal," *Journal of Solid State Chemistry*, vol. 177, no. 10, pp. 3839–3842, 2004.

[11] G. Thomson, *Forensic Application of Raman Spectroscopy*, The University of Leeds, Leeds, UK, 2002.

[12] F. Ikumapayi, M. Makitalo, B. Johansson, and K. H. Rao, "Recycling of process water in sulphide flotation: effect of calcium and sulphate ions on flotation of galena," *Minerals Engineering*, vol. 39, pp. 77–88, 2012.

[13] S. C. Atkinson, *Crystal structures and phase transition in the rare earth oxides [Doctor of Philosophy]*, University of Salford, Salford, UK, 2013.

[14] V. D. Araújo, W. Avansi, H. B. de Carvalho et al., "CeO_2 nanoparticles synthesized by a microwave-assisted hydrothermal method: evolution from nanospheres to nanorods," *CrystEngComm*, vol. 14, no. 3, pp. 1150–1154, 2012.

[15] S. Dogra, J. Singh, N. D. Sharma et al., "Phase progression via phonon modes in lanthanide dioxides under pressure," *Vibrational Spectroscopy*, vol. 70, pp. 193–199, 2014.

[16] J. H. Denning and S. D. Ross, "The vibrational spectra and structures of rare earth oxides in the A modification," *Journal of Physics C: Solid State Physics*, vol. 5, no. 11, article 008, pp. 1123–1133, 1972.

[17] Z. K. Heiba, M. B. Mohamed, and H. Fuess, "XRD, IR, and Raman investigations of structural properties of $Dy_{2-x}Ho_xO_3$ prepared by sol gel procedure," *Crystal Research and Technology*, vol. 47, no. 5, pp. 535–540, 2012.

[18] J. Yu, L. Cui, H. He, S. Yan, Y. Hu, and H. Wu, "Raman spectra of RE_2O_3 (RE=Eu, Gd, Dy, Ho, Er, Tm, Yb, Lu, Sc and Y): laser-excited luminescence and trace impurity analysis," *Journal of Rare Earths*, vol. 32, no. 1, pp. 1–4, 2014.

[19] J. E. Spanier, R. D. Robinson, F. Zhang, S.-W. Chan, and I. P. Herman, "Size-dependent properties of CeO_{2-y} nanoparticles as studied by Raman scattering," *Physical Review B*, vol. 64, no. 24, Article ID 245407, 8 pages, 2001.

[20] D. G. Mead and G. R. Wilkinson, "The temperature dependence of the Raman spectra of some alkaline earth crystals with the fluorite structure," *Journal of Physics C: Solid State Physics*, vol. 10, no. 7, pp. 1063–1072, 1977.

[21] R. C. Stoneman and L. Esterowitz, "Efficient resonantly pumped 2.8-um Er^{3+}: GSGG laser," *Optical Letter*, vol. 17, pp. 816–818, 1992.

[22] Z. H. Wu, D. L. Sun, S. Z. Wang et al., "Performance of a 967 nm CW diode end-pumped Er:GSGG laser at 2.79 μm," *Laser Physics*, vol. 23, no. 5, Article ID 055801, 2013.

[23] P. G. Kik, *Energy transfer in erbium doped optical waveguides based on silicon [Ph.D. Thesis]*, Institute for Atomic and Molecular Physics, Amsterdam, The Netherlands, 2000.

[24] J. K. Krebs and U. Happek, "Yb^{3+} energy levels in α-Al_2O_3," *Journal of Luminescence*, vol. 94-95, pp. 65–68, 2001.

[25] H. A. Eick, L. Eyring, E. Summerville, and R. T. Tuenge, "Electron beam-induced reduction of higher oxides of the rare earths: a high-resolution electron microscopic study," *Journal of Solid State Chemistry*, vol. 42, no. 1, pp. 47–74, 1982.

[26] Z. C. Kang and L. Eyring, "Dynamic edge and surface processes in terbium oxide," *Ultramicroscopy*, vol. 22, no. 1–4, pp. 71–79, 1987.